

Article

# Temperature Sensing of Stepped-Metal Coated Optical Fiber Bragg Grating with the Restructured Dual-Peak Resonance

Yan Feng <sup>1,2,\*</sup> , Ehsan Toyserkani <sup>2</sup>, Hua Zhang <sup>1</sup> and Zhi-Dong Zhang <sup>2</sup>

<sup>1</sup> Key Lab for Robot & Welding Automation of Jiangxi Province, School of Mechatronic Engineering, Nanchang University, Nanchang 330031, Jiangxi, China; zhanghua\_phd@163.com

<sup>2</sup> Multi-Scale Additive Manufacturing Laboratory, Department of Mechanical & Mechatronics Engineering, University of Waterloo, Waterloo, ON N2L 3G1, Canada; ehsan.toyserkani@uwaterloo.ca (E.T.); z496zhang@uwaterloo.ca (Z.-D.Z.)

\* Correspondence: fengyan76@ncu.edu.cn; Tel.: +86-139-7099-2727

Received: 19 December 2018; Accepted: 11 January 2019; Published: 15 January 2019



**Abstract:** This paper demonstrates a method for the development of stepped-metal coating on optical fiber Bragg grating. The paper also analyzes the dual-peak resonance restructured by the nickel/copper stepped-metal coating. According to the coefficients of linear thermal expansion of the coatings, the modeling and experimental analysis is categorized into three types: Type A, Type B, and Type C. We denote the temperature sensitivity difference between the two peaks as  $\Delta K_T$  for Type A,  $\Delta K'_T$  for Type B, and  $\Delta K''_T$  for Type C. The experimental results show that  $\Delta K_T$ ,  $\Delta K'_T$ , and  $\Delta K''_T$  are 2.1 pm/°C, 6.5 pm/°C, and 0.8 pm/°C, respectively. The model analysis and the experimental results all show the Type B stepped-metal coating causes the most obvious temperature sensitivity difference between the two resonance peaks. The stepped-metal coating on the same one Bragg grating can restructure the single resonance into dual-peak resonance with different temperature sensing, and Type B can be used to develop a dual-parameter optical fiber Bragg grating sensor at one location which can measure two physical parameters simultaneously.

**Keywords:** optical fiber Bragg grating; stepped-metal coating; temperature sensing; restructured dual-peak resonance

## 1. Introduction

Optical fiber Bragg grating (FBG) sensing technology has become one of the most attractive sensing technologies in a variety of fields, such as the optical fiber smart structures [1–4]. FBG offers many advantages, such as wavelength encoded nature, wavelength-division multiplexing, immunity to electric–magnetic interference, and small size, etc. FBG is fragile, thus, is required to be protected before its practical use. Previous studies have demonstrated the protective packages can function as parameter compensations [5–8]. During the FBGs actual use period, the birefringence is induced when FBGs are bent, clamped or twisted [9–12]. As a result, the corresponding two Bragg spectra are shown in the reflection spectrum. This might reduce the accuracy of measuring the principal strain and, therefore, be considered as a noise signal. But on the other hand, the dual-peak resonance will provide an opportunity to develop the sensor with the capability of measuring both strain and temperature simultaneously using one optical fiber Bragg grating. Other studies of simultaneous measurement of strain and temperature using birefringence FBGs have been conducted [13–15].

Metal coatings can protect FBG and also enhance their temperature sensitivity and have attracted considerable interest [16–18]. However, there have been few reports about the metallized FBGs'

dual-peak resonance restructured by thermal strains induced by stepped-metal coating on the same Bragg length.

This paper describes the experimental evaluation of the temperature sensing of the single-mode FBG with the Ni/Cu stepped-metal coating by electroless-plating and electroplating. The simulation models analyze the dual-peak resonance restructured by thermal strains and demonstrate the influence of the coating parameters on the two peaks. This kind of optical fiber Bragg grating can be used for a dual-parameter sensor at one location which can measure two physical parameters simultaneously.

## 2. Experimental Set-Up and Results

In the experiments, three FBGs were inscribed in the single mode fibers SMF-128 by UV phase mask with a nominal resonance wavelength of 1541.325 nm, 1539.502 nm, and 1547.835 nm at 25 °C. The length of the Bragg gratings was 10 mm. The stepped-metal coated FBG is hereby expressed as SMC-FBG. We employed a temperature oven (DK-500, Shanghai, China) to control the electroless-plating temperature. Its temperature range is from room temperature to 100 °C, and its temperature resolution is 0.5 °C. And the optical spectrum analyzer (MS9740A, Anritsu, Japan) was used to record the FBGs' data.

### 2.1. First Layer of Inner Metal Coating by Electroless-Plating

Before being electroless-plated, three FBGs were pretreated in sensitizing solution ( $\text{SnCl}_2 \cdot 2\text{H}_2\text{O}$ , 10 g/L; HCl, 40 mL/L) for about ten minutes and then in nucleating solution ( $\text{PdCl}_2$ , 0.5 g/L; HCl, 5 mL/L) for about fifteen minutes. After the pretreatment, the first layer metal coating was deposited on the FBGs by electroless-plating as shown in Figure 1. We chose copper as the first layer of inner metal coating for one FBG and nickel for the other two FBGs. These first layer metal coatings cover the entire length of Bragg grating. The electroless copper plating solution is mainly listed as the following:  $\text{CuSO}_4 \cdot 5\text{H}_2\text{O}$ , 10 g/L;  $\text{NaKC}_4\text{H}_4\text{O}_6 \cdot 4\text{H}_2\text{O}$ , 40 g/L; NaOH, 8 g/L;  $\text{Na}_2\text{CO}_3$ , 2 g/L;  $\text{NiCl}_2 \cdot 6\text{H}_2\text{O}$ , 1 g/L; and HCHO (37%), 20 mL/L. The electroless nickel plating solution is mainly listed as the following:  $\text{NiSO}_4 \cdot 6\text{H}_2\text{O}$ , 25 g/L;  $\text{NaH}_2\text{PO}_2 \cdot \text{H}_2\text{O}$ , 20 g/L;  $\text{H}_3\text{BO}_3$ , 20 g/L; and  $\text{C}_3\text{H}_6\text{O}_2$ , 20 mL/L.

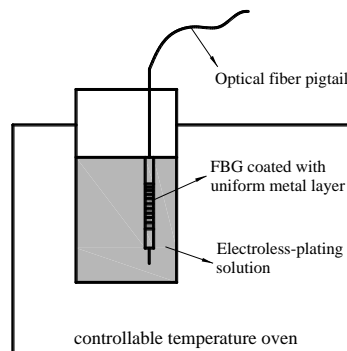


Figure 1. Diagram of electroless-plating.

### 2.2. Second Layer of Outer Stepped-Metal Coating by Electroplating

Figure 2 shows the schematic of the stepped-metal electroplating equipment. Regulating the screw column can control the length of the stepped-metal coating. Different electroplating solutions can develop different packages for this sensor. The SMC-FBGs are divided into three types shown in Figure 3 Type A: a copper layer by electroless-plating and then a stepped-nickel layer by electroplating, Type B: a nickel layer by electroless-plating and then a stepped-copper layer by electroplating and Type C: a nickel layer by electroless-plating and then a stepped-nickel layer by electroplating. The subscript  $i$  ( $i = 1, 2, 3$ ) means FBG, the first layer metal coating and the outer stepped-metal coating, respectively.  $L_i$  refers to the length and  $d_i$  to the diameter. Due to the different deposition rate between the copper layer and nickel layer, deposition time was adjusted to get the same thickness of coatings. For Type A,

it took about three hours to get the inner copper layer and thirteen hours to get the stepped-nickel layer. For Type B, it took about two hours to get the inner nickel layer and fourteen hours to get the stepped-copper layer. For Type C, it took about two hours to get the inner nickel layer and twelve hours to get the stepped-nickel layer. These three types SMC-FBGs are of  $d_1 = 125 \mu\text{m}$ ,  $d_2 = 130 \mu\text{m}$  and  $d_3 = 400 \mu\text{m}$ , respectively. Let  $h_1$  be the thickness of inner uniform metal layer and  $h_2$  be the thickness of outer stepped-metal layer,  $h_1 = (d_2 - d_1)/2$ ,  $h_2 = (d_3 - d_2)/2$ ,  $h_1 = 2.5 \mu\text{m}$ ,  $h_2 = 135 \mu\text{m}$ .

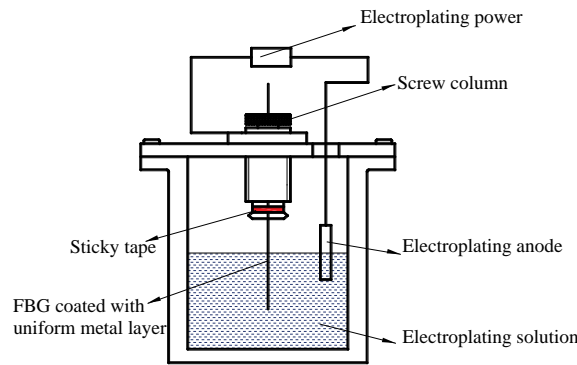


Figure 2. Schematic of the stepped-metal electroplating.

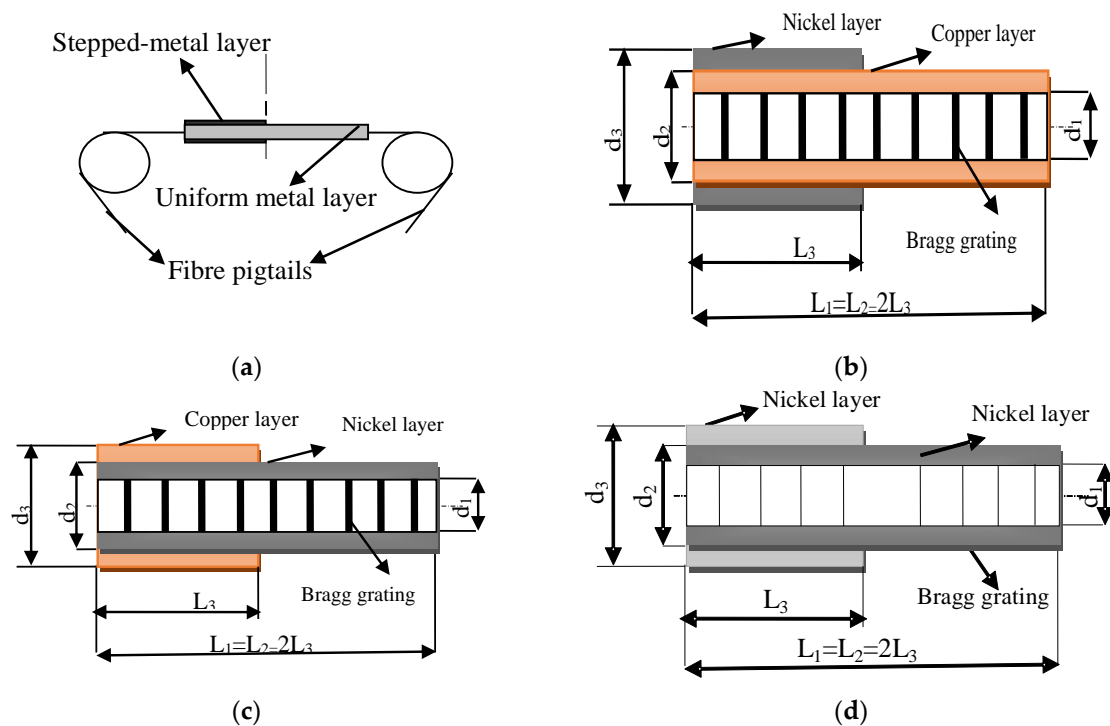
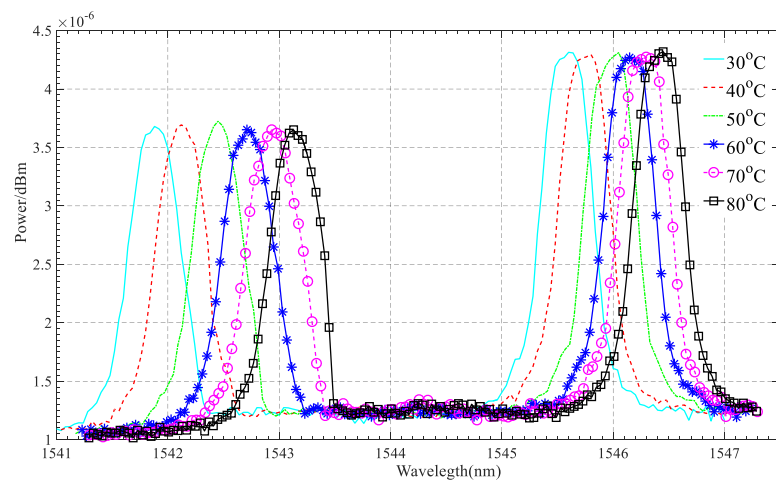


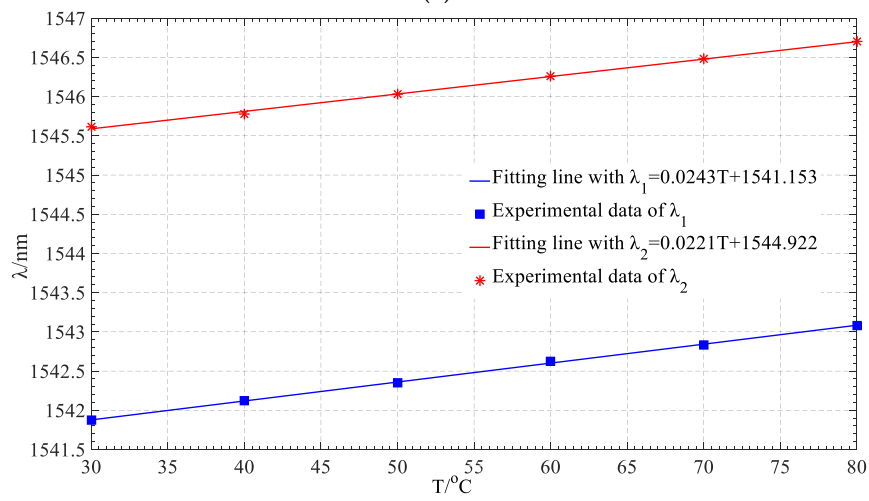
Figure 3. Schematic of the stepped-metal coated-fiber Bragg gratings (SMC-FBGs). (a) appearance diagram, (b) axisymmetric diagram of Type A SMC-FBG, (c) axisymmetric diagram of Type B SMC-FBG, (d) axisymmetric diagram of Type C SMC-FBG.

### 2.3. Temperature Sensing of the SMC-FBG (Stepped-Metal Coated Fiber Bragg Grating)

Three SMC-FBGs were tested by the controllable temperature oven with a precision of  $1 \text{ }^\circ\text{C}$ , and their temperature sensing characteristics are shown in Figures 4–6. The spectra of these three SMC-FBGs all split into two resonance peaks with two different temperature sensitivities. We describe the temperature sensitivity difference between the two peaks as  $\Delta K_T$  for Type A,  $\Delta K'_T$  for Type B and  $\Delta K''_T$  for Type C.  $\Delta K_T$ ,  $\Delta K'_T$  and  $\Delta K''_T$  are  $2.1 \text{ pm}/^\circ\text{C}$ ,  $6.5 \text{ pm}/^\circ\text{C}$  and  $0.8 \text{ pm}/^\circ\text{C}$ , respectively.

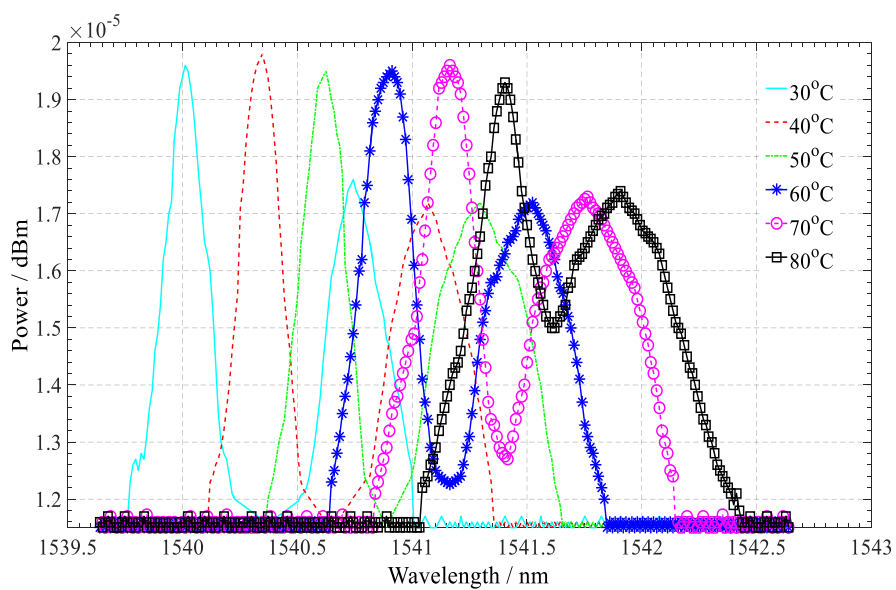


(a)



(b)

Figure 4. Temperature sensing of Type A (a) spectra at 30 to 80  $^{\circ}\text{C}$ . (b) temperature sensitivity.



(a)

Figure 5. Cont.

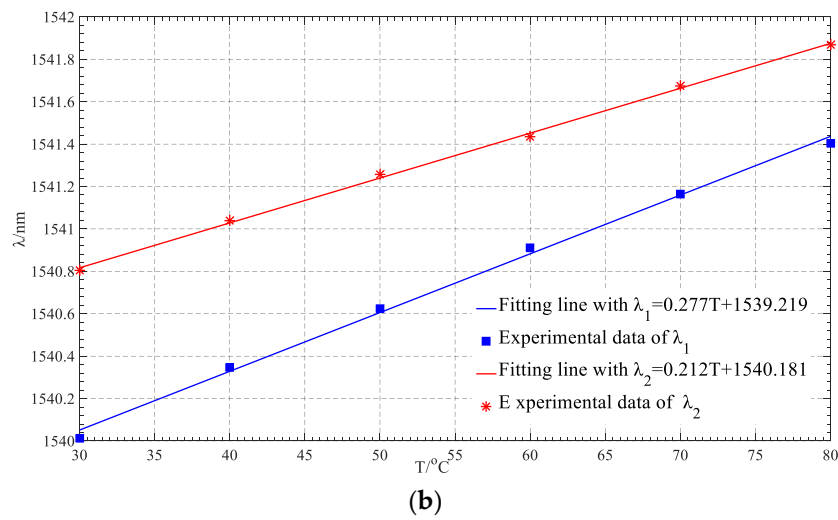


Figure 5. Temperature sensing of Type B (a) spectra at 30 to 80 °C (b) temperature sensitivity.

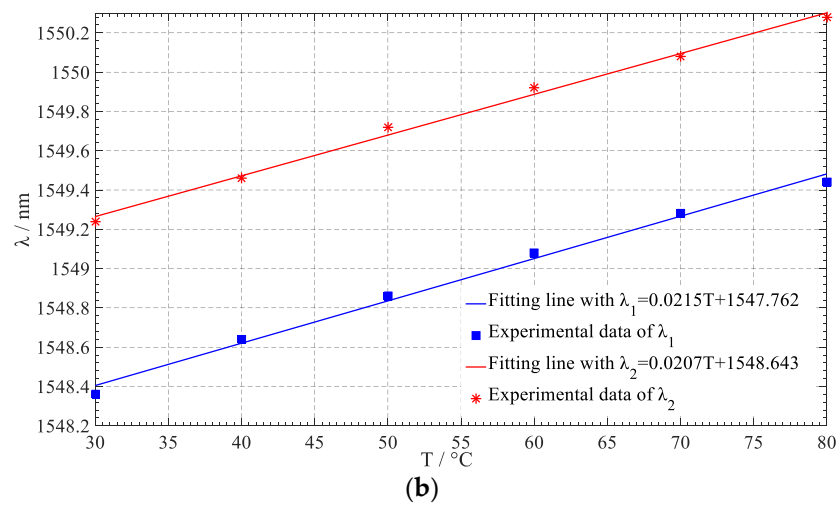
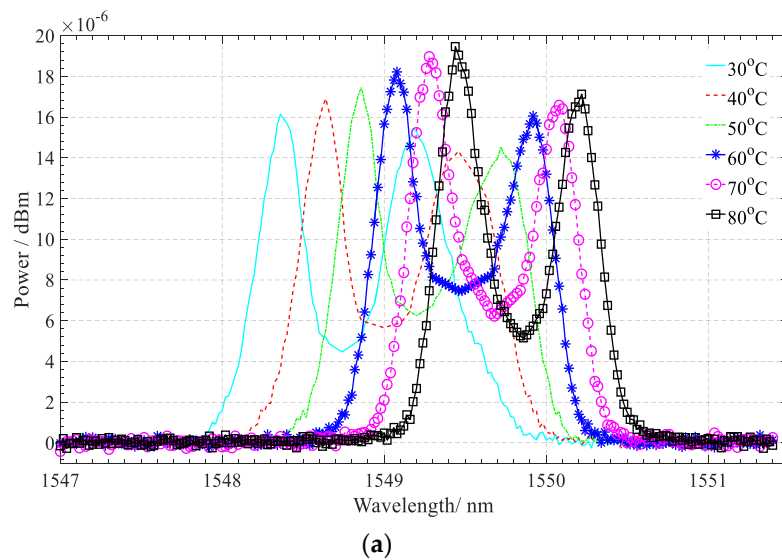


Figure 6. Temperature sensing of Type C (a) spectra at 30 to 80 °C (b) temperature sensitivity.

### 3. Analysis of the Dual-Peak Resonance Restructured by Thermal Strains

In this article,  $\alpha_i$  is used for thermal expansion coefficient,  $E_i$  for Young’s modulus and  $\mu_i$  for Poisson ratio. The model is based on the following assumptions: (1) Thermal expansion coefficients of FBG and the metal coating and thermo-optic coefficient of FBG are constants, independent of temperature changes; (2) The inner metal coating is made on the FBG tightly and; (3) The outer stepped-metal coating and the inner metal coating are attached tightly and there is no relative displacement between them. Three distinct models were developed corresponding to the type of SMC-FBG.

Under strain and temperature, the SMC-FBG’s Bragg wavelength shifts by  $\Delta\lambda_B$  can be expressed as [19]:

$$\Delta\lambda_B = 2n\Lambda \left( \left\{ 1 - \left( \frac{n^2}{2} \right) [p_{12} - \mu(p_{11} + p_{12})] \right\} \varepsilon + \left[ \alpha + \left( \frac{dn}{dT} \right) / n \right] \Delta T \right) \tag{1a}$$

where  $n$  is the effective index of the fiber core,  $\Lambda$  is the grating pitch,  $\alpha$  the coefficient of linear thermal expansion of the fiber,  $p_{i,j}$  are the Pockel’s coefficient of the stress-optic tensor,  $\mu$  is the Poisson’s ratio, and  $\Delta T$  is the temperature change,  $\varepsilon$  is the applied axial strain. The factor  $2n\Lambda$  is the resonance condition of a Bragg grating and expressed as  $\lambda_B$ , the Bragg wavelength. The factor  $\{(n^2/2)[p - \mu(p_{11} + p_{12})]\}$  is usually expressed as  $p_e$ , the Pockels constant. The factor  $[(dn/dT)/n]$  is usually expressed as  $\zeta$ , the thermo-optic coefficients. Equation (1a) can be given simply by Equation (1b).

$$\Delta\lambda_B = \lambda_B(\alpha + \zeta)\Delta T + \lambda_B(1 - p_e)\varepsilon \tag{1b}$$

For an SMC-FBG sensor, the Bragg grating is divided into two sections: double-layer metal coating and single-layer metal coating. Each layer tends to expand or contract when the temperature fluctuates. However, the expansions and contractions generally cannot occur freely due to the boundary limits. Because the restrictions lead to two different thermal strains of the fiber Bragg grating sensor, the dual-peak resonance is induced.

#### 3.1. Analysis of Type A SMC-FBG

Let  $\Delta T > 0$ . Taking Type A as an example, the parameters of coating satisfy  $\alpha_1 < \alpha_3 < \alpha_2$ . Figure 7 shows the diagram of the thermal strains.  $\varepsilon_1 L_1$  is the total thermal strain of FBG, which is caused by the double-layer coating on the half-length of FBG and the single-layer coating on the other half-length of FBG. The letters  $\Delta L_1$ ,  $\Delta L_2$ , and  $\Delta L_3$ , are the free axial elongations of FBG, inner coating and outer coating, respectively, and they can be expressed as Equations (2a)–(2c).

$$\Delta L_1 = \alpha_1 * \Delta T * L_1 \tag{2a}$$

$$\Delta L_2 = \alpha_2 * \Delta T * L_2 \tag{2b}$$

$$\Delta L_3 = \alpha_3 * \Delta T * L_3 \tag{2c}$$

where,  $L_1 = L_2 = 2L_3$ .

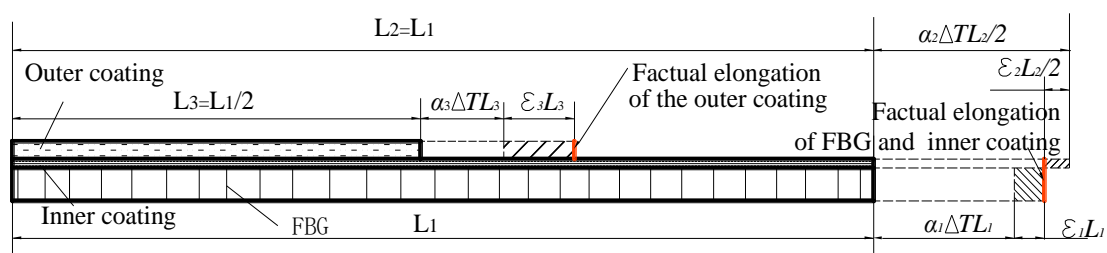


Figure 7. Diagram of the thermal strains of Type A.

### 3.1.1. Wavelength Shift $\Delta\lambda_{dT}$ Caused by the Double-Layer Coating

Because of  $\alpha_1 < \alpha_3 < \alpha_2$  and no relative displacement exists between the inner coating and FBG, the factual elongation of the inner coating will be smaller than  $\Delta L_2$ , the factual elongation of FBG will be greater than  $\Delta L_1$ , and the factual elongation of the outer coating will be greater than  $\Delta L_3$ . At the same time, the thermal stress is satisfied by Equation (3a). The factual elongations of the outer coating, inner coating and FBG are satisfied by Equations (3b) and (3c).

$$\sigma_{d2z}A_2 = \sigma_{d1z}A_1 + \sigma_{d3z}A_3 \tag{3a}$$

$$\alpha_1\Delta T \frac{L_1}{2} + \frac{\sigma_{d1z}}{E_1} \frac{L_1}{2} = \alpha_2\Delta T \frac{L_2}{2} - \frac{\sigma_{d2z}}{E_2} \frac{L_2}{2} \tag{3b}$$

$$\alpha_2\Delta T \frac{L_2}{2} - \frac{\sigma_{d2z}}{E_2} \frac{L_2}{2} = \alpha_3\Delta T L_3 + \frac{\sigma_{d3z}}{E_3} L_3 \tag{3c}$$

where  $\sigma_{diz}$  ( $i = 1, 2, 3$ ) represents the thermal stress of No.  $i$  layer of coating induced by the double-layer coating.  $A_i$  ( $i = 1, 2, 3$ ) is the cross section of No.  $i$  layer. Let  $\varepsilon_{d1z}$  represent the axial thermal strain of the FBG induced by the double-layer coating. From the Equations (3a)–(3c),  $\varepsilon_{d1z}$  can be expressed by Equation (4),

$$\varepsilon_{d1z} = \frac{\sigma_{d1z}}{E_1} = \frac{(E_2A_2 + E_3A_3)(\alpha_2 - \alpha_1)\Delta T - E_3A_3(\alpha_2 - \alpha_3)\Delta T}{E_1A_1 + E_2A_2 + E_3A_3} \tag{4}$$

From Equation (1b), the corresponding wavelength shift  $\Delta\lambda_{dT}$  is expressed using Equation (5)

$$\begin{aligned} \Delta\lambda_{dT} &= \lambda_B(\alpha + \zeta)\Delta T + \lambda_B(1 - p_e)\varepsilon_{d1z} \\ &= \lambda_B * \Delta T \left[ (\alpha + \zeta) + (1 - p_e) * \frac{(E_2A_2 + E_3A_3)(\alpha_2 - \alpha_1) - E_3A_3(\alpha_2 - \alpha_3)}{E_1A_1 + E_2A_2 + E_3A_3} \right] \\ &= K_{dT} * \Delta T \end{aligned} \tag{5}$$

where  $K_{dT}$  is the temperature sensitivity of the SMC-FBG with the double-layer coating.

$$K_{dT} = \lambda_B * \left[ (\alpha + \zeta) + (1 - p_e) * \frac{(E_2A_2 + E_3A_3)(\alpha_2 - \alpha_1) - E_3A_3(\alpha_2 - \alpha_3)}{E_1A_1 + E_2A_2 + E_3A_3} \right] \tag{6}$$

### 3.1.2. Wavelength Shift $\Delta\lambda_{sT}$ Caused by the Single-Layer Coating

The factual elongations of inner layer and FBG are satisfied by the restrictive conditions of Equations (7a) and (7b)

$$\sigma_{s1z}A_1 = \sigma_{s2z}A_2 \tag{7a}$$

$$\alpha_1\Delta T \frac{L_1}{2} + \frac{\sigma_{s1z}}{E_1} \frac{L_1}{2} = \alpha_2\Delta T \frac{L_2}{2} - \frac{\sigma_{s2z}}{E_2} \frac{L_2}{2} \tag{7b}$$

where,  $\sigma_{siz}$  ( $i = 1, 2$ ) represents the thermal stress of No.  $i$  layer of coating induced by the single-layer coating. Then, the thermal strain  $\varepsilon_{s1z}$  is obtained by Equation (8).

$$\varepsilon_{s1z} = \frac{\sigma_{s1z}}{E_1} = \frac{E_2A_2(\alpha_2 - \alpha_1)}{E_1A_1 + E_2A_2} \Delta T \tag{8}$$

The corresponding wavelength shift  $\Delta\lambda_{sT}$  is expressed using Equation (9).

$$\begin{aligned} \Delta\lambda_{sT} &= \lambda_B(\alpha + \zeta)\Delta T + \lambda_B(1 - p_e)\varepsilon_{s1z} \\ &= \lambda_B * \Delta T \left[ (\alpha + \zeta) + (1 - p_e) * \frac{E_2A_2(\alpha_2 - \alpha_1)}{E_1A_1 + E_2A_2} \right] \\ &= K_{sT} * \Delta T \end{aligned} \tag{9}$$



$\sigma''_{diz}$  and  $\sigma''_{siz}$  can be induced by Equations (15a) and (15b). Then the temperature sensitivity  $K''_{dT}$  and  $K''_{sT}$  can be expressed using Equations (16) and (17).

$$\sigma''_{N1z}A_1 = \sigma''_{N2z}A_{N2} \tag{15a}$$

$$\alpha_1\Delta T \frac{L_1}{2} + \frac{\sigma''_{N1z}}{E_1} \frac{L_1}{2} = \alpha_2\Delta T \frac{L_1}{2} - \frac{\sigma'_{N1z}}{E_2} \frac{L_1}{2} \tag{15b}$$

$$K''_{dT} = \lambda_B \left[ (\alpha + \zeta) + (1 - p_e) * \frac{(\alpha_2 - \alpha_1)A_{d2}E_2}{E_2A_{d2} + E_1A_1} \right] \tag{16}$$

$$K''_{sT} = \lambda_B \left[ (\alpha + \zeta) + (1 - p_e) * \frac{(\alpha_2 - \alpha_1)A_{s2}E_2}{E_2A_{s2} + E_1A_1} \right] \tag{17}$$

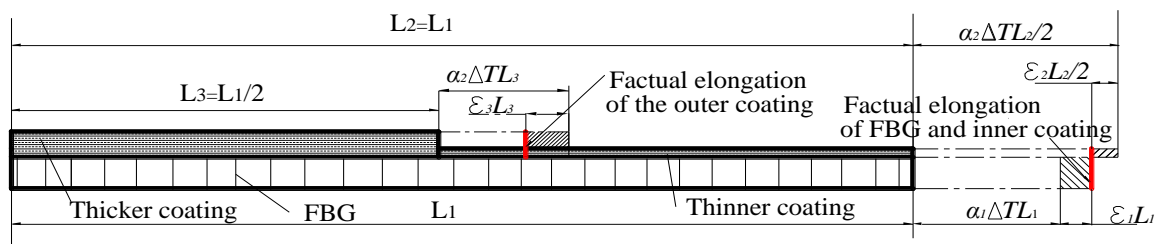


Figure 9. Diagram of the thermal strains of the Type C SMC-FBG.

In three cases, two different strains make the original single reflectance spectrum split into two peaks. Comparing  $K_{sT}$ ,  $K'_{sT}$  and  $K''_{sT}$ , we can find that they are of the same expression with different parameters. We use  $\Delta K_T = K_{dT} - K_{sT}$  to describe the temperature sensing difference between the two peaks for Type A SMC-FBG,  $\Delta K'_T = K'_{dT} - K'_{sT}$  for Type B SMC-FBG, and  $\Delta K''_T = K''_{dT} - K''_{sT}$  for Type C SMC-FBG. Considering  $h_1$  and  $h_2$ ,  $\Delta K_T$  and  $\Delta K'_T$  can be expressed as Equations (18) and (19), whereas, the values of  $\alpha_2$ ,  $\alpha_3$ ,  $E_2$  and  $E_3$  are different. Then  $\Delta K''_T$  can be expressed as Equation (20).

$$\Delta K_T = \lambda_B(1 - p_e) * \left\{ \frac{[E_2h_1(h_1 + d_1) + E_3h_2(2h_1 + d_1 + h_2)](\alpha_2 - \alpha_1) - E_3h_2(2h_1 + d_1 + h_2)(\alpha_2 - \alpha_3)}{E_3h_2(2h_1 + d_1 + h_2) + E_2h_1(h_1 + d_1) + E_1d^2_1} - \frac{E_2h_1(h_1 + d_1)(\alpha_2 - \alpha_1)}{E_2h_1(h_1 + d_1) + E_1d^2_1} \right\} \tag{18}$$

$$\Delta K'_T = \lambda_B(1 - p_e) * \left\{ \frac{E_2h_1(h_1 + d_1)(\alpha_2 - \alpha_1) + E_3h_2(2h_1 + d_1 + h_2)(\alpha_3 - \alpha_1)}{E_3h_2(2h_1 + d_1 + h_2) + E_2h_1(h_1 + d_1) + E_1d^2_1} - \frac{E_2h_1(h_1 + d_1)(\alpha_2 - \alpha_1)}{E_2h_1(h_1 + d_1) + E_1d^2_1} \right\} \tag{19}$$

$$\Delta K''_T = \lambda_B(1 - p_e) * (\alpha_2 - \alpha_1) * E_2 \left\{ \frac{(h_1 + h_2)^2 + d_1(h_1 + h_2)}{E_2[(h_1 + h_2)^2 + d_1(h_1 + h_2)] + E_1d^2_1} - \frac{h_1(h_1 + d_1)}{E_2h_1(h_1 + d_1) + E_1d^2_1} \right\} \tag{20}$$

#### 4. Parametric Analysis

The parameters of the SMC-FBGs are shown in Table 1.

Table 1. Parameters of the stepped-metal coated-fiber Bragg grating (SMC-FBGs).

Parameters \ Type	A	B	C
$\lambda_B$ (nm)	1550	1550	1550
$\alpha_1$ ( $^{\circ}$ C)	$0.55 \times 10^{-6}$	$0.55 \times 10^{-6}$	$0.55 \times 10^{-6}$
$\zeta$ ( $^{\circ}$ C)	$6.3 \times 10^{-6}$	$6.3 \times 10^{-6}$	$6.3 \times 10^{-6}$
$E_1$ (Pa)	$7.4 \times 10^{10}$	$7.4 \times 10^{10}$	$7.4 \times 10^{10}$
$\alpha_2$ ( $^{\circ}$ C)	$17.2 \times 10^{-6}$	$14.2 \times 10^{-6}$	$14.2 \times 10^{-6}$
$E_2$ (Pa)	$10.8 \times 10^{10}$	$19.6 \times 10^{10}$	$19.6 \times 10^{10}$
$\alpha_3$ ( $^{\circ}$ C)	$14.2 \times 10^{-6}$	$17.2 \times 10^{-6}$	$14.2 \times 10^{-6}$
$E_3$ (Pa)	$19.6 \times 10^{10}$	$10.8 \times 10^{10}$	$19.6 \times 10^{10}$

4.1. Analysis of the Temperature Sensitivity

Figure 10 shows the temperature sensing of three types of SMC-FBGs. The following observations can be drawn from Figure 10: (1) If the three types of coating are of the same thickness,  $K''_{dT} < K_{dT} < K'_{dT}$ . (2)  $K_{dT}$  and  $K''_{dT}$  increases with increasing of  $h_1$  at the beginning of increasing of  $h_2$ . Whereas,  $K'_{dT}$  reduces slightly with increasing of  $h_1$  when  $h_2 > 0.18$  mm. (3) When  $h_2$  reaches a certain thickness,  $K_{dT}$ ,  $K'_{dT}$ , and  $K''_{dT}$  will all tend to be constants. (4)  $K'_{sT}$  and  $K''_{sT}$  coincide with each other. (5)  $K_{sT}$ ,  $K'_{sT}$ , and  $K''_{sT}$  all increase with increasing of  $h_1$ . If  $h_1$  is of the same value,  $K_{sT} > K'_{sT} = K''_{sT}$ . When  $h_1$  reaches a certain thickness, they all tend to be constants.

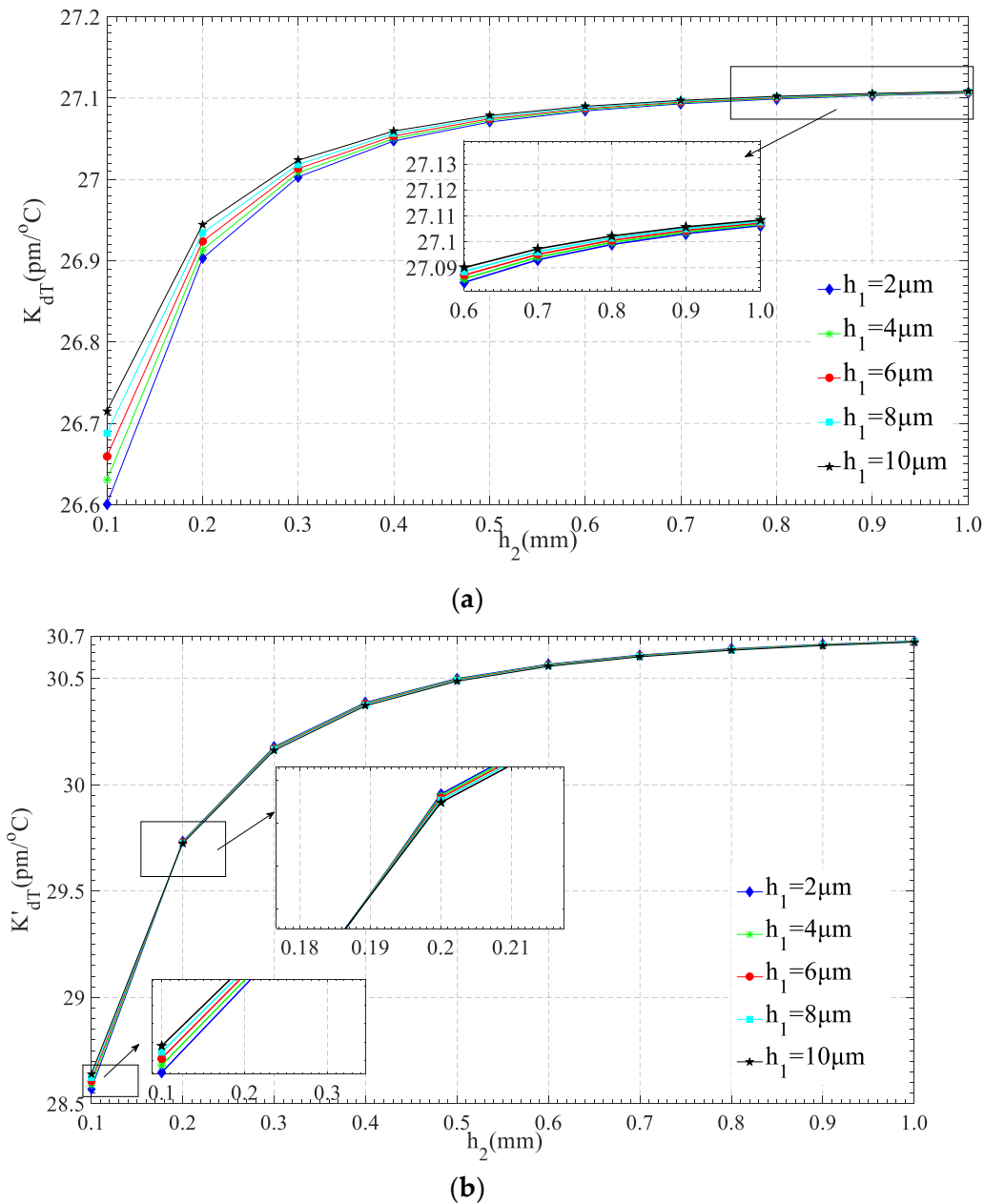
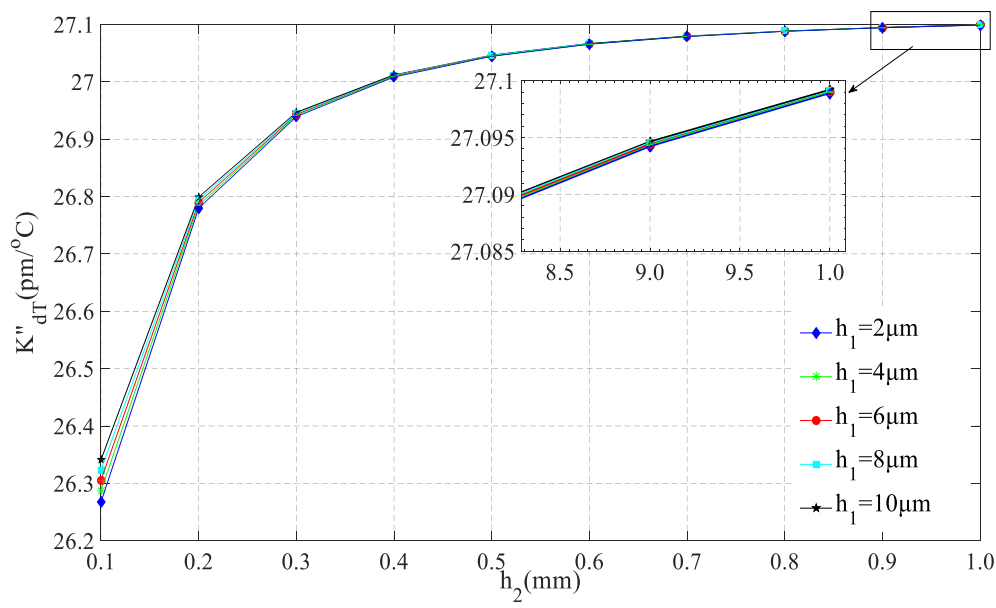
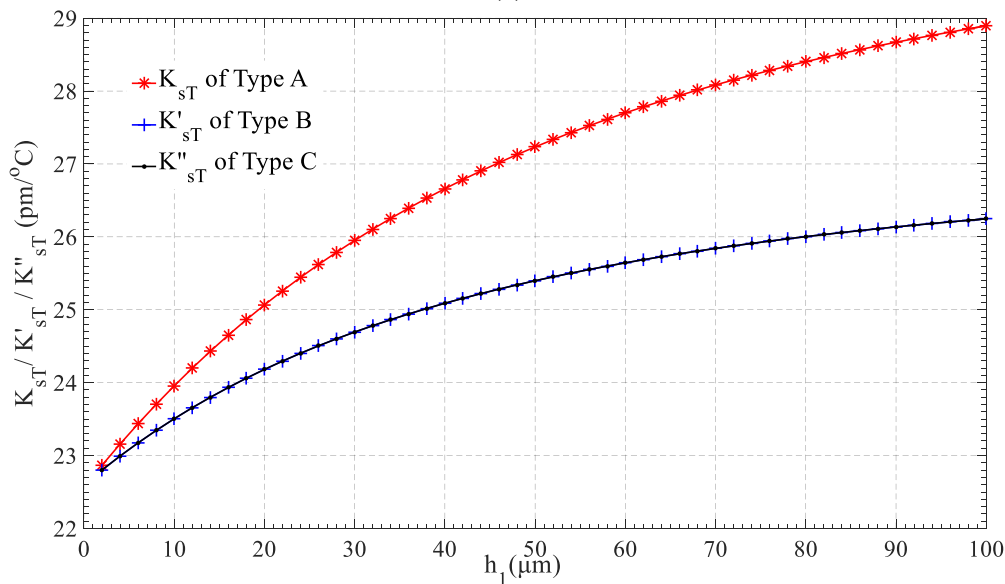


Figure 10. Cont.



(c)



(d)

**Figure 10.** Temperature sensitivity of the SMC-FBGs. (a) double-layer’s  $K_{dT}$  in Type A, (b) double-layer’s  $K'_{dT}$  in Type B (c) double-layer’s  $K''_{dT}$  in Type C, (d) single-layer’s  $K_{sT}$  in Type A,  $K'_{sT}$  in Type B and  $K''_{sT}$  in Type C.

#### 4.2. Analysis of the Temperature Sensitivity Difference

The effect of the coating thickness on the temperature sensitivity difference is shown in Figure 11. We can conclude the followings: (1) When  $h_2$  increases to a certain value, they all tend to be constant values. (2) For the same  $h_2$ ,  $\Delta K_T$ ,  $\Delta K'_T$ , and  $\Delta K''_T$  decrease with the increasing of  $h_1$ . (3)  $\Delta K'_T$  is the largest among them. (4) There is a threshold of  $h_2$  between  $\Delta K_T$  and  $\Delta K''_T$  for every  $h_1 \leq 8 \mu\text{m}$  and  $\Delta K_T > \Delta K''_T$  when  $h_2$  is smaller than this threshold. For example, for  $h_1 = 2 \mu\text{m}$ , the threshold of  $h_2$  is  $200 \mu\text{m}$ .

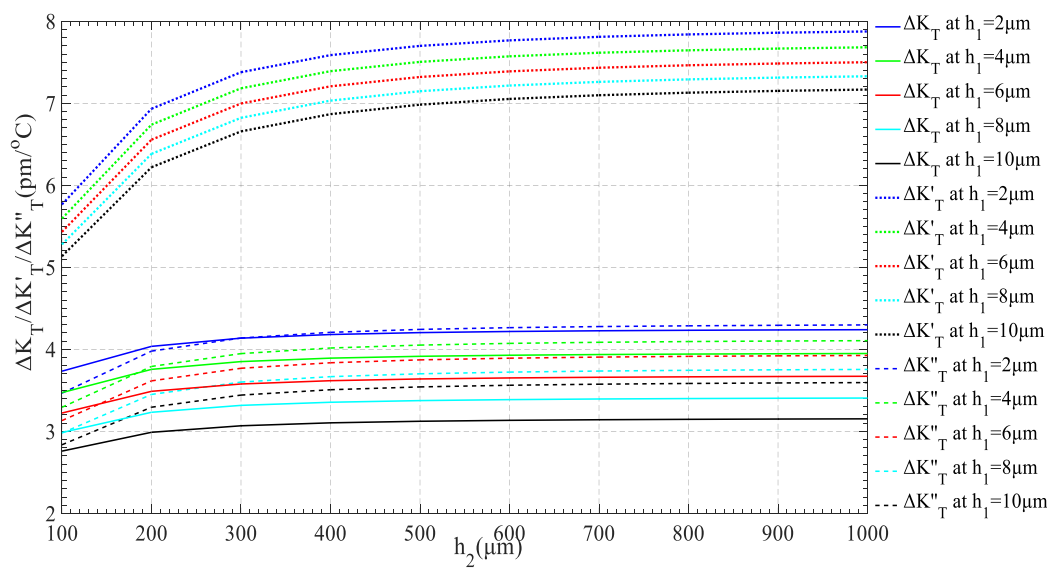


Figure 11. Effects of the coating thickness on  $\Delta K_T$ ,  $\Delta K'_T$  and  $\Delta K''_T$ .

Figure 12 shows the effects of the coating's thermal expansion coefficient on  $\Delta K_T$ ,  $\Delta K'_T$ , and  $\Delta K''_T$ . Under the certain coating thickness (e.g.,  $h_2 = 200 \mu\text{m}$ ,  $h_1 = 5 \mu\text{m}$ ) and Young's modulus,  $\Delta K_T$  and  $\Delta K'_T$  increase with the increase of  $\alpha_3$  when  $\alpha_2$  remains unchanged. Whereas,  $\Delta K_T$  and  $\Delta K'_T$  decrease slightly with the increase of  $\alpha_2$  when  $\alpha_3$  remains unchanged.  $\Delta K''_T$  increases with the increasing of  $\alpha_2$ .

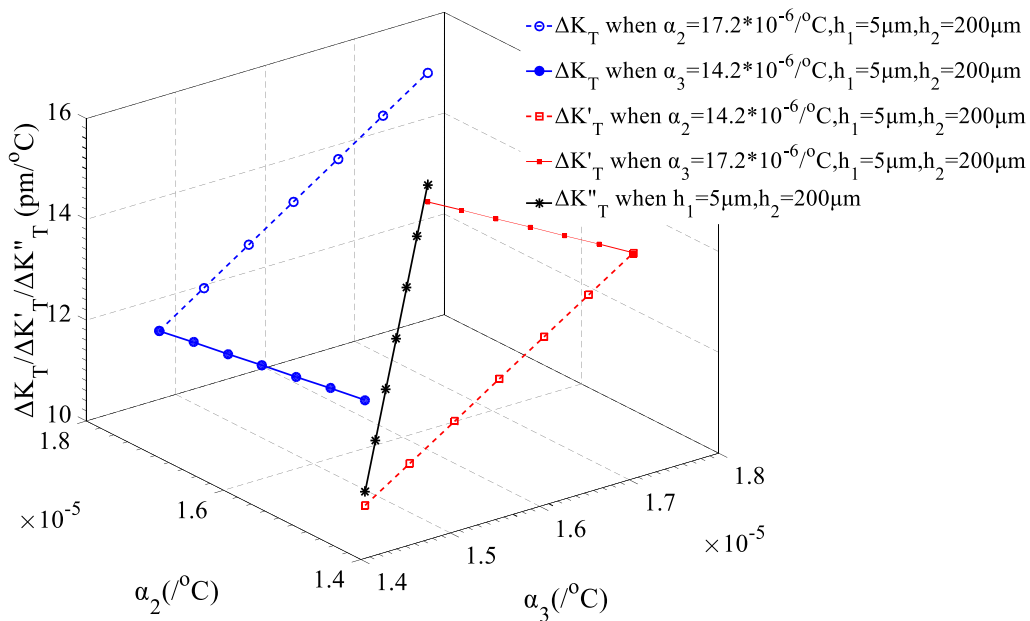


Figure 12. Effects of the coating thermal expansion coefficient on  $\Delta K_T$ ,  $\Delta K'_T$  and  $\Delta K''_T$ .

### 5. Discussion and Conclusions

The two sections of metal layers coated on the same Bragg grating caused two resonance peaks with different temperature sensitivities.

The experimental results show that  $\Delta K''_T < \Delta K_T < \Delta K'_T$ , which is in agreement with the modeling analysis. From the experimental results and the analysis, it can be concluded that Type B SMC-FBG can result in the most obvious difference in the temperature sensitivity between the two resonance peaks among these three type. In Type B, when the outer stepped-metal coating can be successfully plated, with a thinner thickness and a smaller thermal expansion coefficient of the inner coating, and with a

larger thermal expansion coefficient of the outer coating, a more obvious difference of the temperature sensitivity is caused. We can choose another metal material for Type B SMC-FBG to restructure the dual-peak resonance with a much bigger difference between the two peaks, e.g., aluminum/nickel and silver/nickel. This kind of SMC-FBG can be used as a dual-parameter sensor which can measure two physical parameters at one location simultaneously.

On the other hand, the spectrum deformation of Type A is much less than Type B and Type C from the experimental results. We consider that the spectrum deformation is related to the stresses caused by the plating process. We will study this problem in future.

**Author Contributions:** Data curation, Y.F.; Methodology, Y.F.; Project administration, H.Z.; Software, Z.-D.Z.; Validation, E.T.; Writing—original draft, Y.F.; Writing—review & editing, E.T.

**Funding:** This research was funded by the National Natural Science Foundation of China [grant number 51665039].

**Conflicts of Interest:** The authors declare no conflict of interest.

## References

- Xu, R.; Yurkewich, A.; Patel, R.V. Curvature, torsion, and force sensing in continuum robots using helically wrapped FBG sensors. *IEEE Robotics Autom. Lett.* **2016**, *1*, 1052–1059. [[CrossRef](#)]
- Kumar, J.; Prakash, O.; Agrawal, S.K.; Mahakud, R.; Mokhariwale, A.; Dixit, S.K.; Nakhe, S.V. Distributed fiber Bragg grating sensor for multipoint temperature monitoring up to 500 °C in high-electromagnetic interference environment. *Opt. Eng.* **2016**, *55*, 090502. [[CrossRef](#)]
- Da Silva, A.F.; Gonçalves, A.F.; Mendes, P.M. FBG sensing glove for monitoring hand posture. *IEEE Sens. J.* **2011**, *11*, 2442–2448. [[CrossRef](#)]
- Roesthuis, R.J.; Kemp, M.; Van den Dobbelsteen, J.J.; Misra, S. Three-dimensional needle shape reconstruction using an array of fiber Bragg grating sensors. *IEEE/ASME Trans. Mechatron.* **2014**, *19*, 1115–1126. [[CrossRef](#)]
- Khan, M.M.; Panwar, N.; Dhawan, R. Modified cantilever beam shaped FBG based accelerometer with self temperature compensation. *Sens. Actuators A Phys.* **2014**, *205*, 79–85. [[CrossRef](#)]
- Li, J.Z.; Sun, B.C.; Du, Y.L. Union self-compensated packaging of FBG strain sensor. *Optoelectron. Lett.* **2014**, *10*, 30–33. [[CrossRef](#)]
- Prasad, A.G.; Asokan, S. Fiber bragg grating sensor package for submicron level displacement measurements. *Exp. Tech.* **2015**, *39*, 19–24. [[CrossRef](#)]
- Li, Y.; Feng, Y.; Peng, X.; Zhang, H. Simultaneous measurement of the temperature and force using a steel cantilever soldered with a partially nickel coated in-fiber Bragg grating. *Opt. Commun.* **2012**, *285*, 4275–4279. [[CrossRef](#)]
- Wada, D.; Murayama, H. Analytical investigation of response of birefringent fiber Bragg grating sensors in distributed monitoring system based on optical frequency domain reflectometry. *Opt. Lasers Eng.* **2014**, *52*, 99–105. [[CrossRef](#)]
- Lee, J.R.; Tsuda, H.; Koo, B.Y. Single-mode fiber optic Bragg grating sensing on the base of birefringence in surface-mounting and embedding applications. *Opt. Laser Technol.* **2007**, *39*, 157–164. [[CrossRef](#)]
- Tan, R.X.; Ho, D.; Tse, C.H.; Tan, Y.C.; Yoo, S.W.; Tjin, S.C.; Lbsen, M. Birefringent Bragg Grating in C-Shaped Optical Fiber as a Temperature-Insensitive Refractometer. *Sensors* **2018**, *18*, 3285. [[CrossRef](#)] [[PubMed](#)]
- Su, Y.; Zhang, B.; Zhu, Y.; Li, Y. Sensing circular birefringence by polarization-dependent parameters in fibre Bragg gratings and the influence of linear birefringence. *Opt. Fiber Technol.* **2012**, *18*, 51–57. [[CrossRef](#)]
- Chehura, E.; Buggy, S.J.; James, S.; Johnstone, A.; Lakrimi, M.; Domptail, F.; Twin, A.; Tatam, R.; Skordos, A.A. Multi-component strain development in superconducting magnet coils monitored using fiber Bragg grating sensors fabricated in highly linearly birefringent fiber. In Proceedings of the SPIE, Smart Sensor Phenomena, Technology, Networks, and Systems Integration, San Diego, CA, USA, 10–14 March 2013; Volume 8693, p. 86930F.
- Wang, Y.; Huang, X.; Wang, Y. Temperature-insensitive transverse load sensing with improved accuracy using stress induced birefringence effects of fiber Bragg grating. *Opt. Int. J. Light Electron Opt.* **2011**, *122*, 1914–1917. [[CrossRef](#)]
- Luyckx, G.; Voet, E.; Lammens, N.; De Waele, W.; Degrieck, J. Residual strain-induced birefringent FBGs for multi-axial strain monitoring of CFRP composite laminates. *NDT E Int.* **2013**, *54*, 142–150. [[CrossRef](#)]

16. Wang, X.; Dong, X.; Zhou, Y.; Li, Y.; Cheng, J.; Chen, Z. Optical fibre anemometer using silver-coated fiber Bragg grating and bitaper. *Sens. Actuators A Chem.* **2014**, *214*, 230–233. [[CrossRef](#)]
17. Zhang, X.; Alemohammad, H.; Toyserkani, E. Sensitivity alteration of fiber Bragg grating sensors with additive micro-scale bi-material coatings. *Meas. Sci. Technol.* **2013**, *24*, 025106. [[CrossRef](#)]
18. Feng, Y.; Zhang, H.; Li, Y.L.; Rao, C.F. Temperature sensing of metal coated fiber Bragg grating. *IEEE Trans. Mechatron.* **2010**, *15*, 511–519. [[CrossRef](#)]
19. Kersey, A.D.; Davis, M.A.; Patrick, H.J.; LeBlanc, M.; Koo, K.P.; Askins, C.G.; Friebele, E.J. Fiber grating sensors. *J. Lightwave Technol.* **1997**, *15*, 1442–1463. [[CrossRef](#)]



© 2019 by the authors. Licensee MDPI, Basel, Switzerland. This article is an open access article distributed under the terms and conditions of the Creative Commons Attribution (CC BY) license (<http://creativecommons.org/licenses/by/4.0/>).